Modeling and Control of Fuel Cell Based Distributed Generation Systems in a Standalone AC Power Supply

Jin-Woo Jung,[1] **Ali Keyhani,**[2]

1. Samsung SDI Co. Korea
2. Dept. of Electrical and computer Eng. Ohio State University, Columbus, USA

Abstract: This paper develops a circuit model and controllers of fuel cell based distributed generation systems (DGS) in a standalone AC power supply. Dynamic model of the fuel cell is considered. To boost low output DC voltage of the fuel cell to high DC voltage and compensate for its slow response during the transient, two full-bridge DC to DC converters are adopted and their controllers are designed: a unidirectional full-bridge DC to DC boost converter for the fuel cell and a bidirectional full-bridge DC to DC buck/boost converter for the battery. For a three-phase DC to AC inverter, a discrete-time state space model in the stationary dq reference frame is derived and two discrete-time sliding mode controllers are designed: voltage controller in the outer loop and current controller in the inner loop. To demonstrate the proposed circuit model and control strategies, a simulation test-bed using Matlab/Simulink is developed and various results are given.

Keywords: Distributed generation systems, standalone, fuel cells, dynamic modeling, isolated full-bridge DC to DC power converter, three-phase PWM inverter, sliding-mode control.

1. INTRODUCTION

Environmental-friendly distributed generation systems (DGS) such as fuel cells, wind turbines, hydro turbines or photovoltaic arrays are rapidly increasing around the world because they can meet both the increasing demand of electric power and environmental regulations due to green house gas emission [1]-[8]. Outstanding advances in Power Electronics and energy storage devices for transient backup have accelerated penetration of the DGS into electric power generation plants.

These DGS technologies can be used for various applications to a standalone, a grid-interconnection, a cogeneration, a standby, peak shavings, etc. and have many benefits such as environmental-friendly, modular electric generation, increased reliability, high power quality, uninterruptible power service, cost savings, on-site generation, and expandability, etc.

The fuel cells are electrochemical devices which convert chemical energy directly into electric energy by reaction of hydrogen from the fuel and oxygen from the air without regard to climate conditions unlike hydro or wind turbines and photovoltaic arrays [7]-[18], [25]-[26]. Thus, the fuel cells are one of the most attractive DGS resources for power delivery. However, batteries need to be placed in parallel or series with the fuel cell as a temporary energy storage element to support start-up or sudden load changes because the fuel cells can not immediately respond to such abrupt load changes.

For practical analysis of the fuel cell systems, a physical/chemical model [7]-[12] or a first/second order model [13], [14] is used to realize the slow dynamics of the fuel cells. However, most of the papers have not addressed in detail power converter design and control. For single-phase residential applications, the fuel cell is modeled by a DC voltage source to design low-cost and small-sized power converters [15]-[18]. A unidirectional isolated full-bridge DC to DC power converter can be used to boost low fuel cell voltage [19]-[24]. In addition, a bidirectional full-bridge DC to DC power converter can be used for stepping up low battery voltage or stepping down high-voltage-side DC link according to battery discharge or recharge mode [25], [26].

Sedghisigarchi and Feliachi [7], [8] have addressed the fuel-cell dynamic model, and control and stability of the grid-connected DGS, but their two-part paper deals with only PI controllers and does not have energy storage

devices for transient backup. Also, a three-phase PWM inverter is not considered in these papers.

Also, techniques to produce a sinusoidal AC output voltage with low total harmonic distortion (THD) in a three-phase PWM inverter have been reported [27]-[30]. Particularly, even if real-time deadbeat controllers [27]-[29] have low THD for linear load and a fast transient response for load disturbances, it is known that they are sensitive to parametric variations and model uncertainties as well as these techniques have a high THD under nonlinear load. On the other hand, discrete-time optimal voltage/current controllers in a rotating reference frame have been proposed for UPS applications of a three-phase PWM inverter [30]. However, it does not consider a nonlinear load.

The papers stated previously are oriented toward only one part of either dynamic modeling of the fuel cell or design of power converters with a constant DC voltage source such as a forward/push-pull DC to DC boost converter, a single unidirectional full-bridge DC to DC power converter or a single bidirectional full-bridge DC to DC power converter as well as a three-phase DC to AC inverter.

In this paper, simulation studies which cover all the slow dynamics of the fuel cell, a voltage-current polarization curve of the stack, a unidirectional full-bridge boost converter for the fuel cell, a bidirectional full-bridge buck/boost DC to DC power converter for the battery, and a three-phase DC to AC inverter are performed for the fuel-cell-powered DGS to put the battery in parallel to the fuel cell in a standalone AC power supply.

Especially, to boost low output DC voltage of the fuel cell to high DC voltage and compensate for its slow response during the transient, two full-bridge DC to DC converters are adopted and an adaptive proportional controller is designed. For a three-phase DC to AC inverter, two discrete-time sliding mode controllers are designed to guarantee the good performance such as nearly zero steady state inverter output voltage error, low THD, good voltage regulation, robustness, fast transient response, and protection of the inverter against overload under linear/nonlinear loads. To demonstrate the proposed circuit model and control strategies, a simulation test-bed using Matlab/Simulink is developed for the standalone AC power generation with a three-phase AC 120 V/60 Hz/50 kVA.

The paper is organized as follows. Section II illustrates fuel cell based distributed generation systems in a standalone AC power plant. Dynamic model of the fuel cell is shown in Section III. Section IV explains unidirectional/bidirectional full-bridge DC to DC power converters for the fuel cell and battery. Circuit model of DC to AC inverter is given in Section V. Section VI presents control system design. Simulation results of full-bridge DC to DC power converters with dynamics of the fuel cell and three-phase DC to AC inverter are shown in Section VII.

2. FUEL CELL BASED DISTRIBUTED GENERATION SYSTEMS IN A STANDALONE AC POWER SUPPLY

The fuel cell can not immediately respond to power demand during start-up or sudden load changes due to its slow dynamics. As a result, energy storage elements such as batteries or flywheels deliver the remaining power to the load for the transient.

Fuel cell stack voltage, battery position and topology of DC to DC boost converters can be selected variously according to the designers [15]-[18]. In this paper, a low voltage DC output of the fuel cell is used along with the unidirectional boost converter to avoid reliability deterioration by stacking a number of series cells. A low voltage battery for backup is connected in parallel to the high-voltage-side DC bus through a bidirectional buck/boost converter because difficulties in battery management can be significantly reduced. In addition, an isolated full-bridge DC to DC power converter is chosen to boost low output DC voltage of the fuel cell because its topology is suitable for high power applications.

Based on the DGS unit with the battery in parallel to the fuel cell, two applications are promising in industry as illustrated in Fig. 1: a standalone AC power supply and a grid-interconnection.

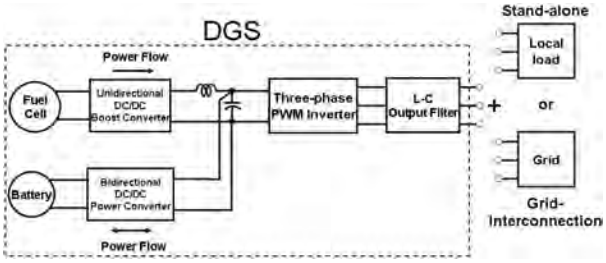

Fig. 1: Configuration for two applications.

In this paper, a standalone operation of two applications above is investigated. Fig. 2 depicts a configuration of the DGS with parallelly connected fuel cell and battery for the standalone AC power plant. It consists of a fuel cell, a battery, unidirectional and bidirectional isolated full-bridge DC to DC power converters, a three-phase DC to AC inverter, an L-C output filter, and a three-phase local load.

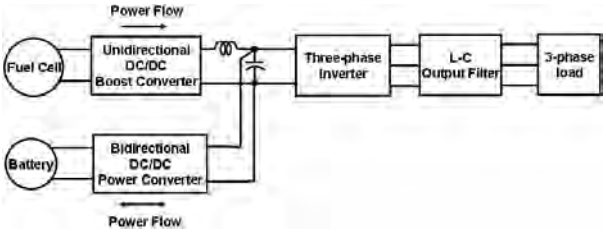

Fig. 2: Configuration of fuel cell based DGS in a standalone AC power supply.

Fig. 3 shows a real system diagram of the DGS that consists of a reformer, stack, a fuel processor controller, a unidirectional boost converter, a bidirectional buck/boost converter, a 3-phase DC to AC inverter, a supervisory controller, two DSP controllers, and a 3-phase load in the standalone AC power generation.

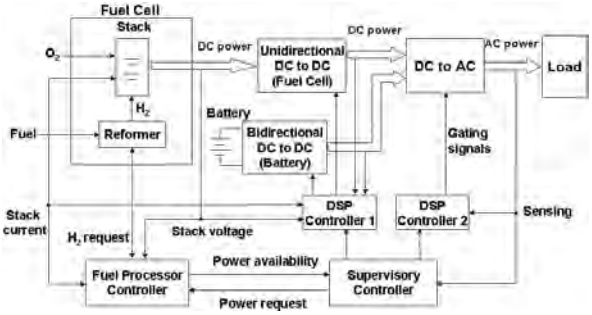

Fig. 3: Detailed system diagram of the DGS with fuel cell and battery.

As described in Fig. 3, the fuel processor controller controls the reformer to produce hydrogen for the power requested from the supervisory controller, and monitors the stack current and voltage. The supervisory controller communicates with the fuel cell processor controller to equalize the power available from the stack to the power requested by the load, and to coordinate protections of the fuel cell. Also, it controls the DSP controller 1 and 2 for the DC and AC power regulation with sensed output voltages/currents. The DSP controller 1 supervises the gating signals of unidirectional and bidirectional DC to DC power converters, and the DSP controller 2 regulates the gating signals of the three-phase DC to AC inverter.

3. MODELING OF FUEL CELL

Among several types of the fuel cells categorized by the electrolyte used, four types are promising for distributed generation systems: Phosphoric Acid fuel cell (PAFC), Solid Oxide fuel cell (SOFC), Molten Carbonate fuel cell (MCFC), Proton-Exchange-Membrane fuel cell (PEMFC).

All types of the fuel cells produce electricity by electrochemical reaction of hydrogen and oxygen, and the oxygen can be easily obtained from compressing air. On the contrary, hydrogen gas required to produce DC power is indirectly gained from the reformer using fuels such as natural gas, propane, methanol, gasoline or from the electrolysis of water.

A typical configuration of an autonomous fuel cell system is described in Fig. 4. As shown in this figure, the fuel cell plants consist of three main parts: a reformer, stack, and power conditioning unit (PCU). First, the reformer produces hydrogen gas from fuels and then provides it for the stack. Second, the stack has many unit cells in series to generate a higher voltage needed for their applications because a single cell that consists of electrolyte, separators, and plates, produces approximately 0.7 V DC. Last, the PCU including power converters convert a low voltage DC from the fuel cell to a high voltage DC and/or a sinusoidal AC.

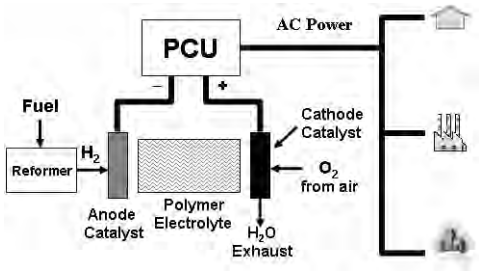

Fig. 4: Configuration of the fuel cell system.

A. Dynamics of Reformer

For dynamic modeling of the fuel cells, the reformer and stack, which determine the dynamic response of the fuel cell system, are further described. Fig. 5 shows a detailed block diagram of the fuel cell system to illustrate its operation.

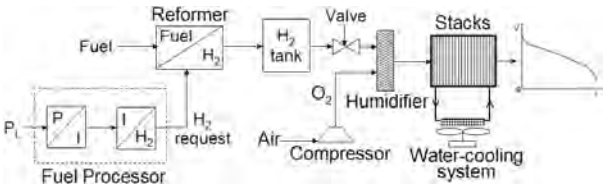

Fig. 5: Detailed block diagram of the fuel cell system.

As depicted in Fig. 5, the fuel cell system consists of fuel cell stack and auxiliary systems such as a fuel cell processor to request the hydrogen gas, a reformer, an air compressor to provide pressurized oxygen flow through the cathode, a valve to control the hydrogen flow through the anode, a humidifier to add moisture to the hydrogen and oxygen gases, and a water-cooling system to remove heat from the stack.

Among the auxiliary systems stated above, the reformer significantly affects the dynamic behavior of the fuel cell system because it takes several minutes to tens of seconds to convert the fuel into the hydrogen depending on the demand of the load current as illustrated in Fig. 6. Thus, to investigate an overall operation of fuel cell powered systems, the dynamics of the reformer need to be considered, and it may be represented by a second order transfer function model [13] or a first order time delay model [14]. In this paper, a first order transfer function is used for the dynamic model of the reformer.

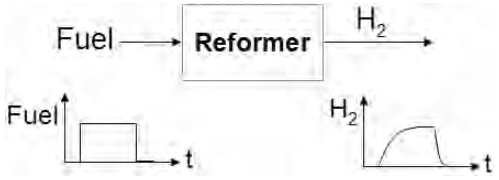

Fig. 6: Dynamic model of the reformer.

B. Voltage-Current Polarization Curve of Fuel Cell Stack

The response of the stack that produces electric DC power from hydrogen and oxygen is much faster than that of the reformer. A voltage-current polarization curve of a fuel cell stack represented in Fig. 7 also needs to be considered for the practical model of the fuel cell. That is, cell voltage decreases as the stack current increases.

Fig. 7 shows a static voltage-current characteristic curve of a single fuel cell. As illustrated in the figure, there exist three regions: region of activation polarization, region of ohmic polarization, and region of concentration polarization. First, in region of activation polarization, the cell voltage drops rapidly with even small current increase. Second, in region of ohmic polarization, the cell voltage linearly decreases as current increases, and the fuel cell normally operates in this region. Last, in region of concentration polarization, the voltage collapses sharply when current exceed the upper limit of safe operation, and as a consequence, operation in this region should be avoided because the fuel cell may be damaged due to primarily starvation of the hydrogen.

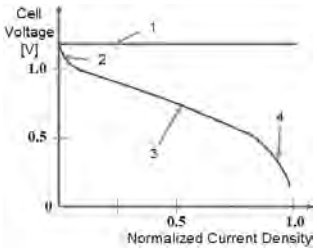

Fig. 7: V-I polarization curve of a single fuel cell.

1. Theoretical EMF or ideal voltage (1.16 V)
2. Region of Activation Polarization (Reaction Rate Loss)
3. Region of Ohmic Polarization
4. Region of Concentration Polarization (Gas Transport Loss)

In this paper, the Proton Exchange Membrane (PEM) Fuel Cells of four promising fuel cells are investigated. Based on an electrochemical process in [10], a Simulink model is developed for the V-I polarization curve of the fuel cell stack as illustrated in Fig. 8.

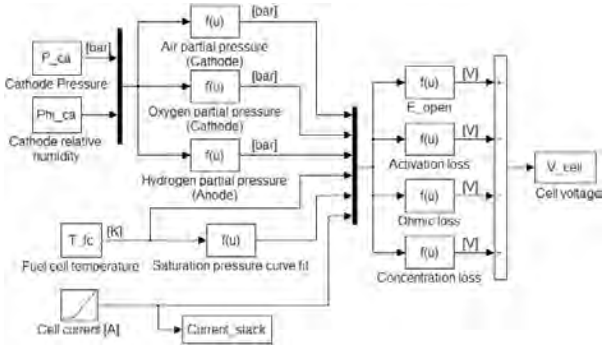

Fig. 8: Simulink model for V-I polarization curve.

In this figure, the polarization curve of the fuel cell is generated using regression models with current, fuel cell temperature, vapor saturation pressure, and oxygen and hydrogen partial pressures. In particular, the oxygen and hydrogen pressures can be estimated from cathode pressure, cathode relative humidity and vapor saturation pressure.

To obtain the voltage-current polarization curve of the fuel cell stack, the following assumptions are made:

- Fuel cell temperature is 80 C at all times.
- Gas distribution is uniform.
- Anode relative humidity is equal to cathode relative humidity and the value is 75%.
- The ratio of pressures between the interior and exterior of the channel is large enough for orifice to be choked.

- The Nernst's equation is applied.
- The cell utilization is 85%.

Based on the above assumptions, the polarization curves of the stack of 250 cells in series for various cathode pressures [1, 1.2, 1.4, 1.6, 1.8, 2 bar] are shown in Fig. 9. As represented in this figure, the linearized polarization curve corresponding to cathode pressure (p_{ca}) of 1.2 bar is selected for a 50 kW PEM fuel cell and it will be used for Simulink model of the fuel cell stack.

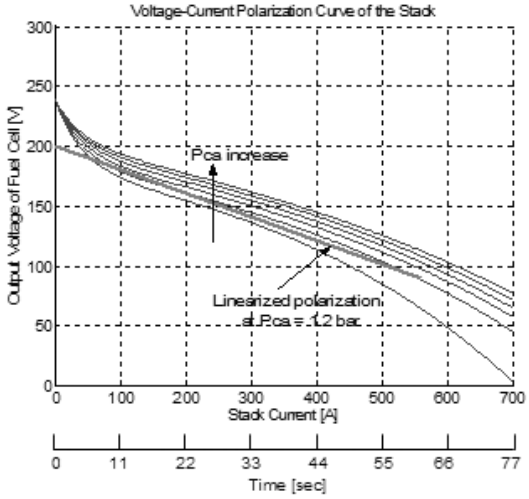

Fig. 9: V-I polarization curves at different cathode pressures (pca).

Note that the fuel cell has the slow dynamic response during transient. At initial startup, it takes 90 seconds for the fuel cell to reach steady state. Whenever there is a change in power demand, the fuel cell takes 60 seconds to reach a new steady state because the hydrogen flow rates can be slowly adjusted to meet the power demand [15]-[18]. To compensate for such a sluggish response of the fuel cell, an energy storage device such as a battery may be required to achieve the end-use needs. For a 50 kW PEM fuel cell, this implies that during startup (90 sec), the energy storage requirement is 4500 kJ or 1.25 kWh. Furthermore, dynamic load changes should be supported by the batteries for 60 seconds. For lead-acid batteries, about 20 % change of nominal charge state may be reasonable to avoid deep discharge and guarantee long service life as well as reserve capacity in the case of an extended fault with the fuel cell. Fig. 10 shows a discharge curve of fuel cell and battery to determine the battery capacity. Considering only 20 % discharge of the nominal battery charge state for 90 seconds (startup), the minimum storage requirement of the batteries to support the fuel cell during all transients is about 22,500 kJ or 6.25 kWh.

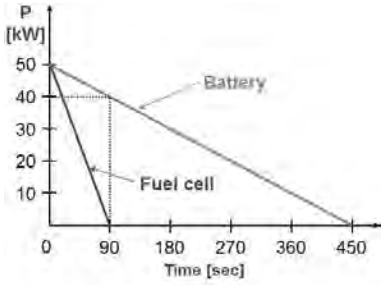

Fig. 10: Discharge curve of fuel cell and battery.

5. UNIDIRECTIONAL/BIDIRECTIONAL FULL-BRIDGE DC TO DC POWER CONVERTERS

To boost low output DC voltage of the fuel cell to high DC voltage, a forward DC to DC boost converter, a push-pull DC to DC boost converter or an isolated full-bridge DC to DC power converter can be selected. Among these power converters, two phase-shifted full-bridge DC to DC converters, which are one of the most attractive topologies for high power generation [19]-[26], are adopted as described in Fig. 11: a unidirectional full-bridge DC to DC boost converter for the fuel cell and a bidirectional full-bridge DC to DC boost/buck converter for battery.

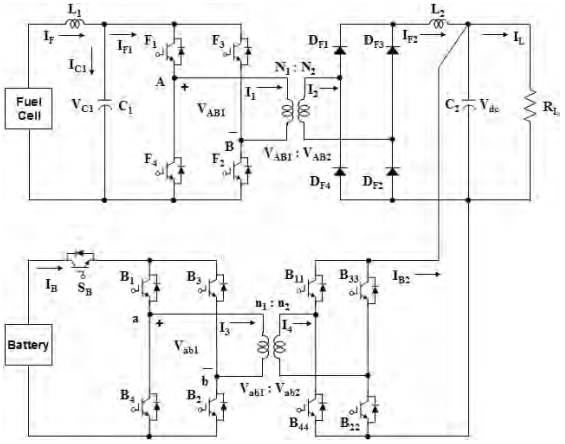

Fig. 11: Unidirectional/bidirectional DC to DC power converters.

In Fig. 11, the unidirectional power converter system for the fuel cell consists of a fuel cell, an input filter (L_1, C_1), a full-bridge power converter "1" (F_1 to F_4), a high frequency transformer (N_1:N_2), a bridge-diode (D_{F1} to D_{F4}), and an output filter (L_2, C_2), while the bidirectional power converter system for the battery consists of a battery, a static switch (SB), two full-bridge power converter "2" (B_1 to B_4) and "3" (B_{11} to B_{44}), and a high

frequency transformer (n_1:n_2).

Fig. 12 shows power flows of DC to DC power converters for battery discharge and battery recharge. As shown in Fig. 12, the unidirectional full-bridge DC to DC boost converter permits only one directional power flow from the fuel cell to the load because a reverse current can damage the fuel cell, and a response speed of the power converter should be slow enough to meet slow dynamic response of the fuel cell. On the other hand, the bidirectional full-bridge DC to DC power converter allows both directional power flows for battery discharge and recharge, and its response also should be fast to compensate for the slow dynamics of the fuel cell during start-up or sudden load changes.

For battery discharge mode illustrated in Fig. 12 (a), which occurs when a startup or a sudden load increase, the fuel cell starts delivering electric power to the load and the battery instantly provides power until the fuel cell reaches a full operation state. After transient operation, only the fuel cell feeds electric power to the load. For battery recharge mode shown in Fig. 12 (b), the battery absorbs the energy overflowed from the fuel cell to prevent DC-link voltage V_{DC} from being overcharged during a sudden load decrease, and then the battery is recharged by the fuel cell in a steady-state until it reaches a nominal voltage.

(a)

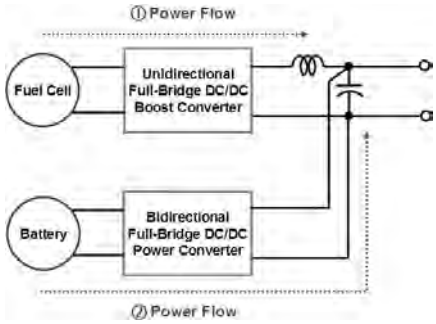

(b)

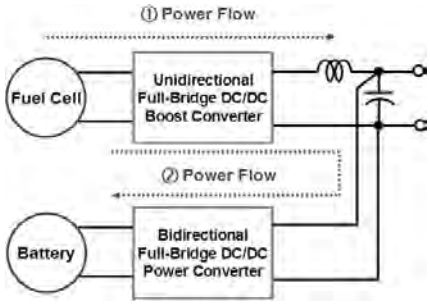

Fig. 12: Power flows of DC to DC power converters. (a) Battery discharge. (b) Battery recharge.

6. THREE-PHASE DC TO AC INVERTER

A circuit model of a three-phase DC to AC inverter with L/C output filter is further described in Fig. 13. As shown in the figure, the system consists of a DC voltage source (V_{dc}), a three-phase PWM inverter (S1 to S6), an output filter (L_f and C_f), and a three-phase load (RL). Note that the first stage of DGS that consists of a fuel cell, a battery, and two full-bridge DC to DC power converters is replaced with the DC voltage source (V_{dc}) because during transient the battery fully supports the fuel cell with a slow dynamic response to keep the DC-link voltage (V_{dc}) constant and as a result, the first stage can be considered as a stiff DC energy source.

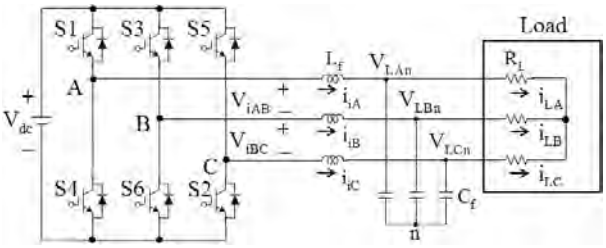

Fig. 13: Three-phase DC to AC inverter with L-C output filter.

The circuit model described in Fig. 13 uses the following quantities. The inverter output line-to-line voltages and output currents are represented by the vectors $V_i = [V_{iAB}\ V_{iBC}\ V_{iCA}]^T$ and $I_i = [i_{iA}\ i_{iB}\ i_{iC}]^T$. Also, the load line to neutral voltage and phase current vectors can be represented by $V_L = [V_{LAn}\ V_{LBn}\ V_{LCn}]^T$ and $I_L = [i_{LA}\ i_{LB}\ i_{LC}]^T$, respectively.

The L-C output filter yields the following state equations by KCL and KVL:

$$\frac{d\mathbf{V}_L}{dt} = \frac{1}{C_f}\mathbf{I}_i - \frac{1}{C_f}\mathbf{I}_L$$
$$\mathbf{T}_i\frac{d\mathbf{I}_i}{dt} = -\frac{1}{L_f}\mathbf{T}_i\mathbf{V}_L + \frac{1}{L_f}\mathbf{V}_i \qquad (1)$$

where, $\mathbf{T}_i = \begin{bmatrix} 1 & -1 & 0 \\ 0 & 1 & -1 \\ -1 & 0 & 1 \end{bmatrix}$

To implement the space vector PWM, the above state equations can be transformed from the *abc* reference frame into stationary *dq* reference frame that consists of the horizontal (d) and vertical (q) axes. The relation between these two reference frames is below

$$\mathbf{f}_{dq0} = \mathbf{K}_s\mathbf{f}_{abc} \qquad (2)$$

where, $\mathbf{K}_s = \frac{2}{3}\begin{bmatrix} 1 & -1/2 & -1/2 \\ 0 & \sqrt{3}/2 & -\sqrt{3}/2 \\ 1/2 & 1/2 & 1/2 \end{bmatrix}$, $f_{dq0}=[f_d \ f_q \ f_0]^T$, $f_{abc}=[f_a f_b f_c]^T$, and f denotes either a voltage or a current variable.

Using (2), the (1) can be transformed below

$$\frac{d\mathbf{V}_{Ldq}}{dt} = \frac{1}{C_f}\mathbf{I}_{idq} - \frac{1}{C_f}\mathbf{I}_{Ldq}$$
$$, \quad \frac{d\mathbf{I}_{idq}}{dt} = -\frac{1}{L_f}\mathbf{V}_{Ldq} + \frac{1}{L_f}T^{-1}{}_{idq}\mathbf{V}_{idq} \qquad (3)$$

where, $\mathbf{T}^{-1}{}_{idq} = [\mathbf{K}_s\mathbf{T}_i\mathbf{K}_s^{-1}]^{-1} = \frac{1}{2}\begin{bmatrix} 1 & \frac{1}{\sqrt{3}} \\ -\frac{1}{\sqrt{3}} & 1 \end{bmatrix}$.

The given plant model (3) can be expressed as the following continuous-time state space equation

$$, \dot{\mathbf{X}}(t) = \mathbf{A}\mathbf{X}(t) + \mathbf{B}\mathbf{u}(t) + \mathbf{E}\mathbf{d}(t) \qquad (4)$$

where, $\mathbf{X} = \begin{bmatrix} \mathbf{V}_{Ldq} \\ \mathbf{I}_{idq} \end{bmatrix}_{4\times1}$, $\mathbf{A} = \begin{bmatrix} 0_{2\times2} & \frac{1}{C_f}I_{2\times2} \\ -\frac{1}{L_f}I_{2\times2} & 0_{2\times2} \end{bmatrix}_{4\times4}$, $\mathbf{B} = \begin{bmatrix} 0_{2\times2} \\ \frac{1}{L_f}T^{-1}{}_{idq} \end{bmatrix}_{4\times2}$

$$, \mathbf{E} = \begin{bmatrix} -\frac{1}{C_f}I_{2\times2} \\ 0_{2\times2} \end{bmatrix}_{4\times2}, \mathbf{u} = [\mathbf{V}_{idq}]_{2\times1} \ , \mathbf{d} = [\mathbf{I}_{Ldq}]_{2\times1} \ .$$

Note that the load line to neutral voltage V_{Ldq} and inverter output phase current I_{idq} are the state variables, the inverter output line-to-line voltage V_{idq} is the control input (u), and the load phase current I_{Ldq} is defined as the disturbance (d).

7. CONTROL SYSTEM DESIGN

A. Full-Bridge DC to DC Power Converters

Based on the circuit model in Fig. 11, two full-bridge DC to DC power converters have to boost low DC voltage of the fuel cell and battery, and regulate tightly the DC-link voltage (Vdc) to a required voltage in spite of fuel cell output voltage fluctuating according to load. Moreover, a bidirectional DC to DC power converter for the battery should backup the fuel cell with a slow dynamic response during transient behavior.

To realize the factors above, a new topology with a static switch SB on the side of battery which can control both directional power flows is proposed in Fig. 11. Fig. 14 (a) and (b) show waveforms of power transistors for battery discharge and recharge, respectively. As depicted in the figures, a phase-shifted angle (δ) is controlled to meet the power demand and regulate DC-link voltage (V_{dc}) to a desired value.

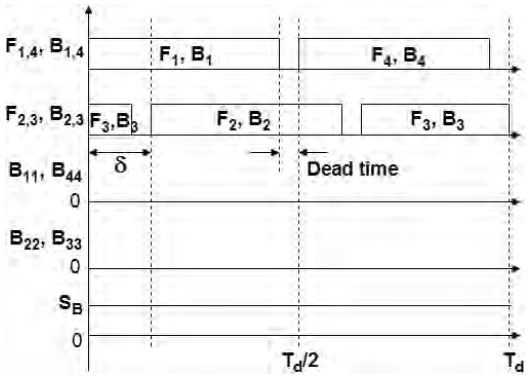

(a)

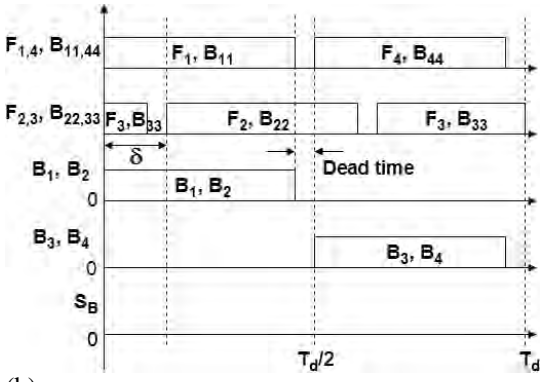

(b)

Fig. 14: Waveforms of power switches for unidirectional/bidirectional DC to DC converters. (a) Battery discharge. (b) Battery recharge.

During start-up or rapid load increase as shown in Fig. 14 (a), the power converters (F_1 to F_4, B_1 to B_4) run as a phase-shifted full-bridge converter and all power switches of the power converter (B_{11} to B_{44}) on the secondary side of battery's transformer are turned off. Additionally, the static switch SB is turned on for the battery to backup the fuel cell during transient.

For rapid load decrease or steady-state as illustrated in

Fig. 14 (b), the power converters (F_1 to F_4, B_{11} to B_{44}) operate as a phase-shifted full-bridge converter, whereas the power converter (B_1 to B_4) on the primary side of battery's transformer acts as a regular PWM full-bridge converter. Also, the static switch S_B is turned off for absorption of overcharged power or battery recharge in steady-state time.

Fig. 15 shows a control block diagram of unidirectional and bidirectional full-bridge DC to DC converters. In Fig. 15, load current IL, fuel cell current IF2 on the high voltage side, battery voltage V_B and DC-link voltage V_{dc} are measured to perform closed-loop control. Note that high frequency components of all measured currents are filtered out by low-pass filter for accurate voltage and current control.

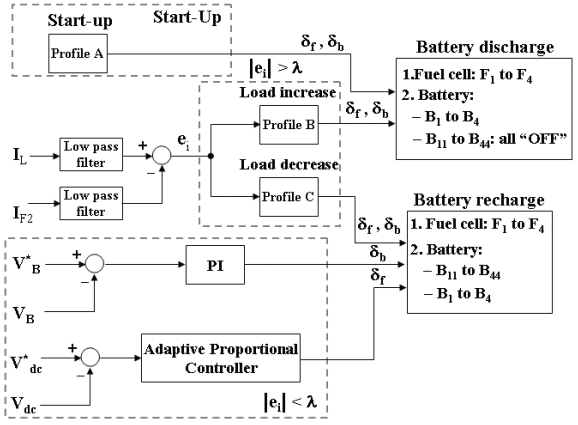

Fig. 15: Control block diagram of DC to DC power converters.

As represented by Fig. 15, control variables of two DC to DC power converters are phase-shifted angels (δ_f, δ_b), where δ_f is a phase-shifted angle for the fuel cell and δ_b is a phase-shifted angle for the battery, and there exist three main loops: start-up, $|e_i| > \lambda$, and $|e_i| < \lambda$, where $e_i = I_L \quad I_{F2}$ and is a small positive value.

During start-up, phase-shifted angles (δ_f, δ_b) of two power converters are given by "Profile A" predetermined for soft starting. For $|e_i| > \lambda$, a difference between a filtered load current (I_L) and a filtered fuel cell current (I_{F2}) is used to determine either "load increase" or "load decrease". The angles are determined by "Profile B" and "Profile C" which meet dynamic characteristics of the fuel cell and battery, depending on load increase or load decrease. If the difference is positive, "Profile B" is selected for the battery to backup the fuel cell. On the other hand, if the difference is negative, "Profile C" is chosen so that the battery can absorb electric energy overflow from the fuel cell due to abrupt load decrease. After $|e_i|$ goes within λ, an adaptive proportional controller is used to regulate the DC-link voltage V_{dc} and a discrete-time PI controller is used to recharge the battery from the fuel cell until the battery voltage V_B reaches a nominal value. The adaptive controller is designed to prevent abrupt switching action which can cause a large amount of current ripple by properly adjusting the gain according to the error between reference DC-link voltage V^*_{dc} and measured voltage V_{dc}. Also, if fuel cell stack current IF and battery current I_B are above the limit which can damage cells, two power converters will shut down.

B. Three-Phase DC to AC Inverter

To supply a qualified AC power to the local load connected to the distributed generation systems (DGS), good performance such as a low THD, a fast transient response, and over-current protection should be guaranteed under linear/nonlinear loads.

Fig. 16 shows a control block diagram of a three-phase DC to AC inverter. As represented by Fig. 16, two discrete-time sliding mode controllers (DSMC) are proposed to perform zero steady state tracking error, THD reduction, and fast and no-overshoot response: current controller in the inner loop and voltage controller in the outer loop. First of all, the DSMC is suitable for digital implementation since it does not exhibit the chattering phenomena due to direct digital implementation of continuous time sliding mode control [31].

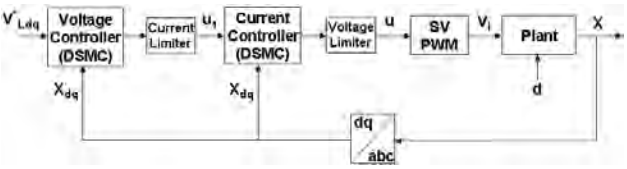

Fig. 16: Control block diagram of a three-phase DC to AC inverter.

1) Current Controller in the Inner Loop

For design of a discrete-time current controller, the continuous-time state space equation (4) of the plant can be transformed to a discrete form:

$$\begin{cases} \mathbf{X}(k+1) = \mathbf{A}^*\mathbf{X}(k) + \mathbf{B}^*\mathbf{u}(k) + \mathbf{E}^*\mathbf{d}(k) \\ \mathbf{y}_1(k) = \mathbf{C}_1\mathbf{X}(k) \\ \mathbf{e}_{idq}(k) = \mathbf{y}_1(k) - \mathbf{y}_{1\_ref}(k) \end{cases}, \qquad (5)$$

where, $\mathbf{y}_1 = [\mathbf{I}_{idq}]$, $\mathbf{y}_{1\_ref} = [\mathbf{I}^*_{idq}]$, $\mathbf{C}_1 = \begin{bmatrix} 0 & 0 & 1 & 0 \\ 0 & 0 & 0 & 1 \end{bmatrix}$, $\mathbf{d} = [\mathbf{I}_{Lqd}]$, $\mathbf{A}^* = e^{\mathbf{A}T_z}$, $\mathbf{B}^* = \int_0^{T_z} e^{\mathbf{A}(T_z-\tau)}\mathbf{B}d\tau$, $\mathbf{E}^* = \int_0^{T_z} e^{\mathbf{A}(T_z-\tau)}\mathbf{E}d\tau$.

In order to control the output y1(k) to follow the reference y1_ref(k), a sliding mode manifold can be selected below

$$\mathbf{s}(k) = \mathbf{y}_1(k) - \mathbf{y}_{1\_ref}(k) = \mathbf{C}_1\mathbf{X}(k) - \mathbf{y}_{1\_ref}(k) \quad . \qquad (6)$$

Therefore, discrete-time sliding mode can be reached if the control input u(k) is designed as the solution of:

$$\mathbf{s}(k+1) = \mathbf{y}_1(k+1) - \mathbf{y}_{1\_ref}(k+1) \, . \qquad (7)$$

The control law that satisfies (7) and yields motion in the manifold s(k) = 0 is called 'equivalent control' and is given:

$$\mathbf{u}_{eq}(k) = \left(\mathbf{C}_1\mathbf{B}^*\right)^{-1}\left(\mathbf{I}^*_{idq}(k) - \mathbf{C}_1\mathbf{A}^*\mathbf{X}(k) - \mathbf{C}_1\mathbf{E}^*\hat{\mathbf{d}}(k)\right). \qquad (8)$$

If the control is limited by $\|\mathbf{u}(k)\| \le u_v$, then the following modified control input can be applied:

$$\mathbf{u}(k) = \begin{cases} \mathbf{u}_{eq}(k) & \text{for } \|\mathbf{u}_{eq}(k)\| \le u_v \\ \dfrac{u_v}{\|\mathbf{u}_{eq}(k)\|}\mathbf{u}_{eq}(k) & \text{for } \|\mathbf{u}_{eq}(k)\| > u_v \end{cases} . \qquad (9)$$

With control law (9), the discrete-time sliding mode can be reached after a finite number of steps and the control voltage limit $\mathbf{u}_0$ is also determined by the SVPWM inverter.

2) Voltage Controller in the Outer Loop

For the dynamics of the DSMC to be included in the outer loop, its model has to be combined with the original plant.

After the dynamics (8) of the DSMC is included in (5), the overall plant can be expressed:

$$\begin{cases} \mathbf{X}(k+1) = \mathbf{A}_d\mathbf{X}(k) + \mathbf{B}_d\mathbf{u}_1(k) + \mathbf{E}_d\mathbf{d}(k) \\ \mathbf{y}(k) = \mathbf{C}_d\mathbf{X}(k) \\ \mathbf{e}_{vdq}(k) = \mathbf{y}(k) - \mathbf{y}_{ref}(k) \end{cases} , \qquad (10)$$

where, $\mathbf{y} = [\mathbf{V}_{Ldq}]$, $\mathbf{C}_d = [I_{2\times2} \quad 0_{2\times2}]$, $\mathbf{A}_d = \mathbf{A}^* - \mathbf{B}^*\left(\mathbf{C}_1\mathbf{B}^*\right)^{-1}\mathbf{C}_1\mathbf{A}^*$, $\mathbf{B}_d = \mathbf{B}^*\left(\mathbf{C}_1\mathbf{B}^*\right)^{-1}$, $\mathbf{E}_d = \mathbf{E}^* - \mathbf{B}^*\left(\mathbf{C}_1\mathbf{B}^*\right)^{-1}\mathbf{C}_1\mathbf{E}^*$, $\mathbf{u}_1(k) = \mathbf{I}_{cmd,idq}(k)$.

To be similar to the current controller, a sliding mode manifold may be chosen in the form of:

$$\mathbf{s}(k) = \mathbf{C}_d\mathbf{X}(k) - \mathbf{y}_{ref}(k) \, . \qquad (11)$$

Thus, if the control input $u_1(k)$ is designed to be the solution of s(k+1)=0, the discrete-time sliding mode can be reached after a finite number of steps and the equivalent control (u_{1eq}) is given by:

$$\mathbf{u}_{1eq}(k) = \left(\mathbf{C}_d\mathbf{B}^*_d\right)^{-1}\left(\mathbf{V}^*_{Ldq}(k) - \mathbf{C}_d\mathbf{A}_d\mathbf{X}(k) - \mathbf{C}_d\mathbf{E}_d\mathbf{d}(k)\right). \qquad (12)$$

If the control is limited by , then the following modified control input can be applied:

$$\mathbf{u}_1(k) = \begin{cases} \mathbf{u}_{1eq}(k) & \text{for } \|\mathbf{u}_{1eq}(k)\| \le u_i \\ \dfrac{u_0}{\|\mathbf{u}_{1eq}(k)\|}\mathbf{u}_{1eq}(k) & \text{for } \|\mathbf{u}_{1eq}(k)\| > u_i \end{cases} . \qquad (13)$$

Note that the control law u_{1eq}(k) is limited by 300% of the rated current.

8. SIMULATION RESULTS

To validate the effectiveness of the fuel cell model and control strategies of full-bridge DC to DC and three-phase DC to AC power converters that are proposed for the fuel cell based distributed generation systems in the standalone AC power plant, a simulation test bed using Matlab/Simulink is constructed for an AC 120 V (L-n)/60 Hz/50 kVA.

In this paper, to overcome an excessive computation time due to three power converters and high PWM frequencies, it is assumed that the dynamic response time of the fuel cell is significantly reduced compared to its normal response time. Also, the simulation test bed is divided into two parts: two full-bridge DC to DC power converters with the dynamic model of the fuel cell and a three-phase DC to AC inverter. It is reasonable if the DC to DC power converters tightly regulate the DC-link bus voltage (V_{dc}) that is used as an input of the three-phase DC to AC inverter within a desired value.

A. Full-Bridge DC to DC Power Converters

To demonstrate the fuel cell model and control scheme presented for two full-bridge DC to DC power converters, a simulation test bed using Matlab/Simulink is developed.

Fig. 17 shows a Simulink model of the fuel cell, and it consists of a power request, a power to current conversion, a first-order transfer function for the transient response of the reformer, a controlled current source, a linearized polarization curve for the modeling of the stack, and a controlled voltage source.

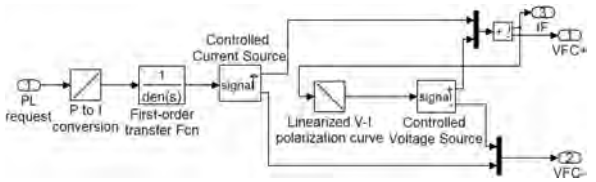

Fig. 17: Simulink model of the fuel cell.

Fig. 18 shows a Simulink model of two full-bridge DC to DC power converters with the fuel cell and the battery, and it consists of a fuel cell, an input filter (L_1 and C_1), a unidirectional isolated full-bridge DC to DC power converter, an output filter (L_2 and C_2), a battery, a static switch (S_B), a bidirectional isolated full-bridge DC to DC power converter, two PWM controllers, and a load. The system parameters are given in Table I.

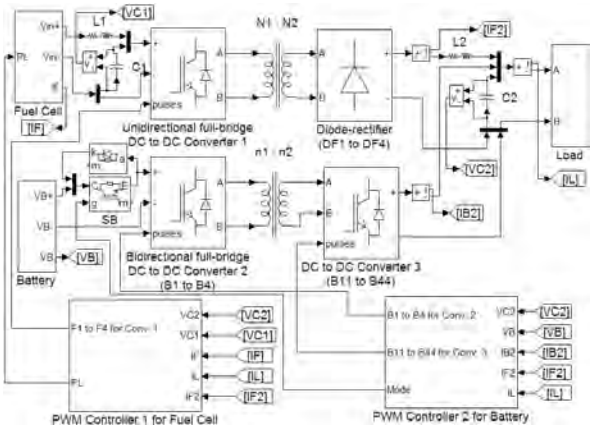

Fig. 18: Simulink model of full-bridge DC to DC power converters with the fuel cell and battery.

TABLE I SYSTEM PARAMETERS

Fuel Cell Output Voltage	88 ~ 200 V
Nominal Battery Voltage	120 V
Turn Ratios (N_1:N_2, n_1:n_2)	1:6.5, 1:6
Input Filters	L_1 = 20 μH, C_1 = 1000 μF
Output Filters	L_2 = 150 μH, C_2 = 10000 μF
Switching Frequency	f_d = 10 kHz
Desired DC Output Voltage	V_{dc} = 500V

To show a general dynamic response of the fuel cell, assume that it takes 12 msec for fuel cell to reach from no-load to full load and takes 4 msec (1/3 of the increasing time) and vice versa [14]. Fig. 19 to 21 show simulation results under startup, a sudden load increase, and a sudden load decrease, respectively.

Each figure indicates: (1) Power request (P), (2) Fuel cell voltage (V_{C1}), (3) Fuel cell current (I_F), (4) Filtered output current (I_{F2}) of fuel cell on DC-link side, (5) Filtered output current (I_{B2}) of battery on DC-link side, and (6) High-side DC-link voltage (V_{dc}).

In Fig. 20, a power request signal is changed from 0 to 20 kW at 42 msec, and then 20 kW to 40 kW at 62 msec. In Fig. 21, the power request signal is changed from 0 to 40 kW at 42 msec, and dropped to 20 kW at 62 msec.

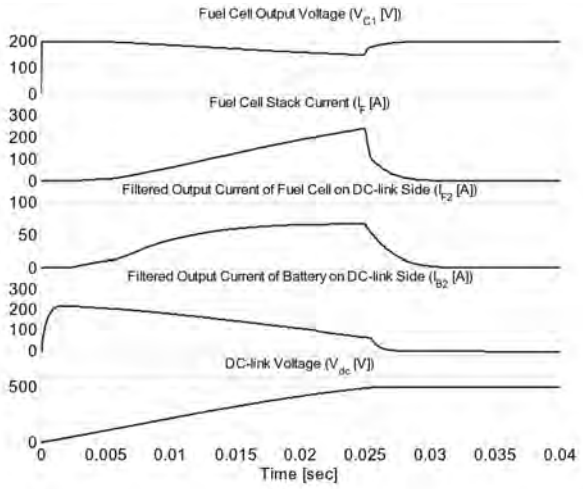

Fig. 19: Simulation waveforms during start-up.

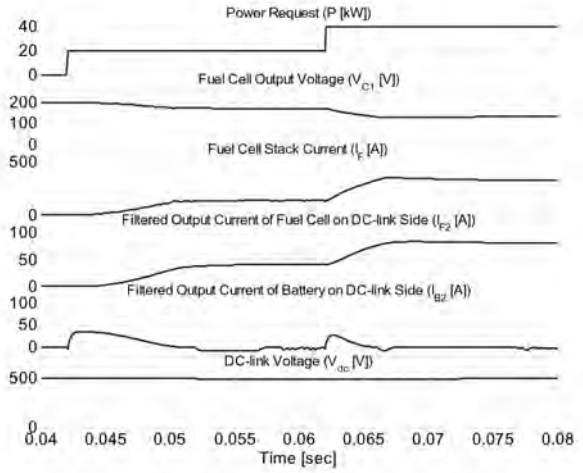

Fig. 20: Simulation waveforms under a sudden load increase.

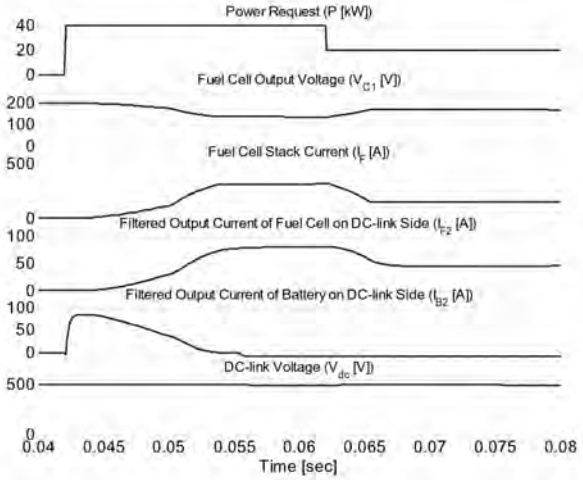

Fig. 21: Simulation waveforms under a sudden load decrease.

As depicted in Fig. 19 to 21, the fuel cell current (IF) has some delay because it takes some time for the fuel to be converted to the hydrogen, which is demanded for the request power, and the fuel cell voltage and current depend on each other as voltage-current polarization curve of the stack.

Also, the DC-link bus (V_{dc}) is nearly constant during the transients because the battery appropriately backs up the fuel cell. The battery is discharged during startup and abrupt load increase, while it slowly recharged by the fuel cell to reach a nominal value during rapid load decrease or in steady-state time.

B. Three-Phase DC to AC Inverter

To validate the control strategy proposed for three-phase DC to AC inverter, a simulation test bed using Matlab/Simulink is constructed as illustrated in Fig. 22, and the system parameters are given in Table II.

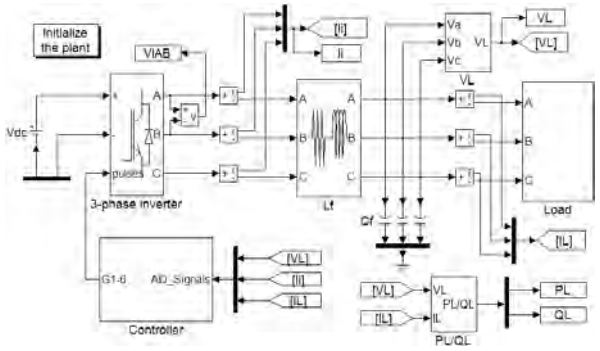

Fig. 22: Simulink model for a 3-phase PWM inverter.

TABLE II SYSTEM PARAMETERS

DC Bus Voltage	V_{dc}= 500 V
Output Power Rating	P_{out} = 50 kVA
AC Output Voltage	$V_{L,RMS}$ = 120 V (L-N), f = 60 Hz
Inverter Filters	L_f = 250 µH, C_f = 580 µF
Switching Frequency	f_s = 9 kHz

Fig. 23 and 24 show the results under a linear load (p.f. = 0.8) and a nonlinear load with a three-phase diode bridge, respectively. In Fig. 25 and 26, the simulation results show a resistive load step change at 50 msec from 0 to 40 kW, and vice versa. Fig. 27 shows simulation results under a resistive unbalanced load, i.e., the phase A and B are normal, while the phase C is open at 50 msec.

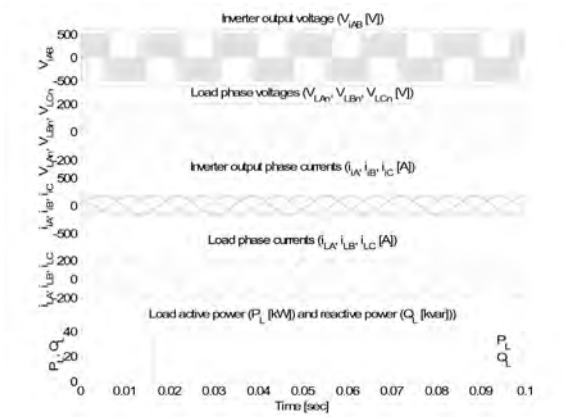

Fig. 23: Results under a linear load (p.f. =0.8).

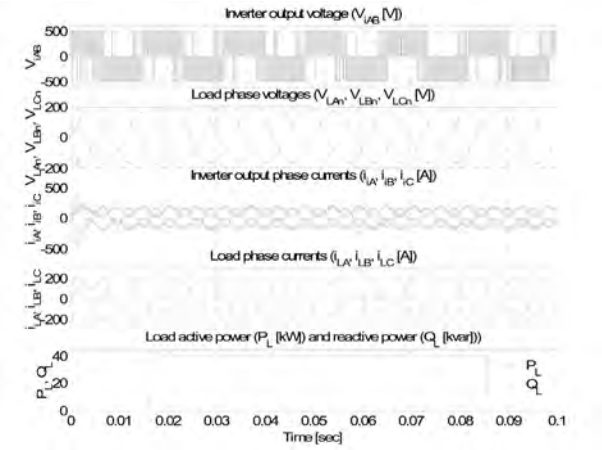

Fig. 24: Results under a nonlinear load.

In Fig. 23 through 27, each figure indicates: (1) Inverter output line to line voltage (V_{iAB}), (2) Load phase voltages (V_{LAn}, V_{LBn}, V_{LCn}), (3) Inverter output phase currents (i_{iA}, i_{iB}, i_{iC}), (4) Load phase currents (i_{LA}, i_{LB}, i_{LC}), and (5) Load active power (P_L) and reactive power (Q_L).

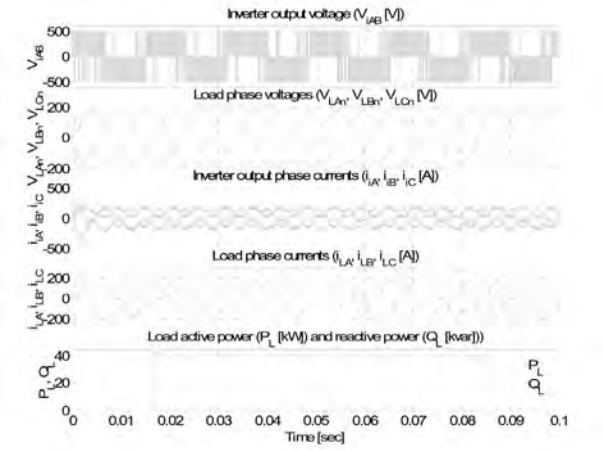

Fig. 25: Results under a resistive balanced load step

change (0 to 40 kW).

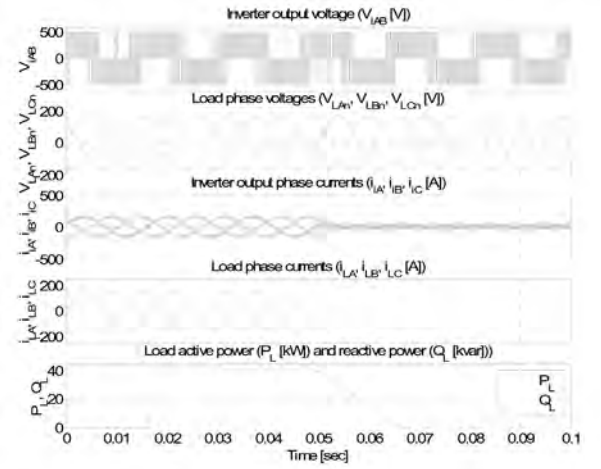

Fig. 26: Results under a resistive balanced load step change (40 kW to 0).

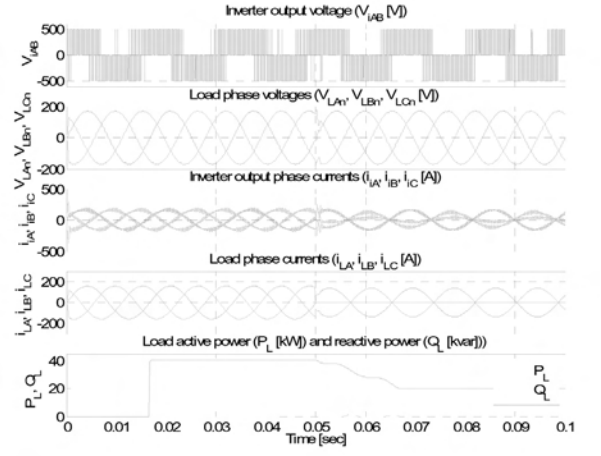

Fig. 27: Results under a resistive unbalanced load (Phase A & B: normal and Phase C: open at 50 msec.).

From Fig. 23 to 27, the proposed control method demonstrates the good performance such as a low THD, a fast transient response, and over-current protection under the linear load, nonlinear load, and even resistive load step changes. Note that it takes 1/60 seconds for the PL and QL to be accurately calculated using Simulink model in the figures.

9. CONCLUSIONS

This paper has described the circuit model and controller design of the fuel-cell-powered DGS to put the battery in parallel to the fuel cell in a standalone AC power supply.

A simulation test-bed using Matlab/Simulink is presented, which includes the dynamic model of the fuel cell, the unidirectional full-bridge DC to DC boost converter (fuel cell), the bidirectional full-bridge DC to DC buck/boost converter (battery), and the three-phase DC to AC inverter.

Especially, a new topology with a static switch on the side of battery which can control both directional power flows is proposed for the bidirectional full-bridge DC to DC buck/boost converter. For three power converters, the controllers are designed: an adaptive proportional controller for two DC to DC power converters and two discrete-time sliding mode controllers for the three-phase DC to AC inverter. From Fig. 19 to 27, the effectiveness of the proposed circuit model and control methods is validated.

ACKNOWLEDGMENT

This work was supported in part by the National Science Foundation under the grant NSF ECE 0501349.

REFERENCES

[1] M. N. Marwali and A. Keyhani, "Control of Distributed Generation Systems, Part I: Voltages and Currents Control," IEEE Transaction on Power Electronics, vol. 19, pp. 1541-1550, Nov. 2004.

[2] M. N. Marwali, J. W. Jung, and A. Keyhani, "Control of Distributed Generation Systems, Part II: Load Sharing Control," IEEE Trans. on Power Electronics, vol. 19, pp. 1551-1561, Nov. 2004.

[3] A. A. Chowdhury, S. K. Agarwal, D. O. Koval, "Reliability modeling of distributed generation in conventional distribution systems planning and analysis," IEEE Transactions on Industry Applications, vol. 39, pp. 1493-1498, Sept.-Oct. 2003.

[4] T. Monai, I. Takano, H. Nishikawa, and Y. Sawada, "Response characteristics and operating methods of new type dispersed power supply system using photovoltaic fuel cell and SMES," IEEE Power Engineering Society Summer Meeting, vol. 2, pp. 874-879, July 2002.

[5] J. L. Del Monaco, "The Role of Distributed Generation in the Critical Electric Power Infrastructure," IEEE-Power Engineering Society Winter Meeting, vol. 1, pp. 144 -145, 2001.

[6] L. Philipson, "Distributed and Dispersed Generation: Addressing the Spectrum of Consumer Needs," IEEE-Power Engineering Society Summer Meeting, vol. 3, pp. 1663 -1665, 2000.

[7] K. Sedghisigarchi and A. Feliachi, "Dynamic and Transient Analysis of Power Distribution Systems With Fuel Cells-Part I: Fuel-Cell Dynamic Model," IEEE Transactions on Energy Conversion, vol. 19, pp. 423-

428, June 2004.
[8] K. Sedghisigarchi and A. Feliachi, "Dynamic and Transient Analysis of Power Distribution Systems With Fuel Cells-Part II: Control and Stability Enhancement," IEEE Transactions on Energy Conversion, vol. 19, pp. 429-434, June 2004.
[9] L.Y. Chiu and B. M. Diong, "An improved small-signal model of the dynamic behavior of PEM fuel cells," IEEE 38th IAS Annual Meeting, vol. 2, pp. 709-715, Oct. 2003.
[10] J. T. Pukrushpan, H. Peng, and A. G. Stefanopoulou, "Simulation and analysis of transient fuel cell system performance based on a dynamic reactant flow model," Proc. of ASME IMECE'02, 2002.
[11] S. Yerramalla, A. Davari, A. Feliachi, "Dynamic modeling and analysis of polymer electrolyte fuel cell," IEEE Power Engineering Society Summer Meeting, vol. 1, pp. 82-86, July 2002.
[12] J. T. Pukrushpan, A. G. Stefanopoulou, and H. Peng, "Modeling and control for PEM fuel cell stack system," American Control Conference, vol. 4, pp. 3117-3122, May 2002.
[13] K. H. Hauer, "Dynamic interaction between the electric drive train and fuel cell system for the case of an indirect methanol fuel cell vehicle,"35th IECEC Meeting, vol. 2 , pp. 1317-1325, July 2000.
[14] Yoon-Ho Kim and Sang-Sun Kim, "An electrical modeling and fuzzy logic control of a fuel cell generation system," IEEE Transactions on Energy Conversion, vol. 14, no. 2, pp. 239-244, June 1999.
[15] G. K. Andersen, C. Klumpner, S. B. Kjaer, and F. Blaabjerg, "A new green power inverter for fuel cells," IEEE PESC'02, vol. 2, pp. 727-733, June 2002.
[16] R. Gopinath, Sangsun Kim, Jae-Hong Hahn, M. Webster, J. Burghardt, S. Campbell, D. Becker, P. Enjeti, M. Yeary, and J. Howze, "Development of a low cost fuel cell inverter system with DSP control," IEEE PESC'02, vol. 1, pp. 309-314, June 2002.
[17] A. M. Tuckey and J. N. Krase, "A low-cost inverter for domestic fuel cell applications,"IEEE PESC'02, vol. 1, pp. 339-346, June 2002.
[18] E. Santi, D. Franzoni, A. Monti, D. Patterson, F. Ponci, and N. Barry, "A fuel cell based domestic uninterruptible power supply," IEEE APEC'02, vol.1, pp. 605-613, March 2002.
[19] A. Bendre, G. Venkataramanan, and D. Divan, "Dynamic analysis of loss-limited switching full-bridge DC-DC converter with multimodal control," IEEE Transactions on Industry Applications, vol. 39, pp. 854-863, 2003.
[20] M. T. Aydemir, A. Bendre, and G. Venkataramanan, "A critical evaluation of high power hard and soft switched isolated DC-DC converters," IEEE IAS'02, vol. 2, pp. 1338-1345, Oct. 2002.
[21] Eun-Soo Kim, Kee-Yeon Joe, Moon-Ho Kye, Yoon-Ho Kim, and Byung-Do Yoon, "An improved ZVZCS PWM FB DC/DC converter using energy recovery snubber," IEEE APEC'97, vol. 2, pp. 1014-1019, Feb. 1997.
[22] P. K. Jain, Wen Kang, H. Soin, and Youhao Xi, "Analysis and design considerations of a load and line independent zero voltage switching full bridge DC/DC converter topology," IEEE Transactions on Power Electronics, vol. 17, pp. 649-657, Sept. 2002.
[23] M. Brunoro and J. L. F. Vieira, "A high-performance ZVS full-bridge DC-DC 0-50-V/0-10-A power supply with phase-shift control," IEEE Transactions on Power Electronics, vol. 14, pp. 495-505, May 1999.
[24] Seong-Jeub Jeon and Gyu-Hyeong Cho, "A zero-voltage and zero-current switching full bridge DC-DC converter with transformer isolation," IEEE Transactions on Power Electronics, vol. 16, pp. 573-580, Sept. 2001.
[25] F. Z. Peng, Hui Li, Gui-Jia Su, and J. S. Lawler, "A new ZVS bidirectional DC-DC converter for fuel cell and battery application," IEEE Trans. on Power Electronics, vol. 19, pp. 54-65, Jan. 2004.
[26] Z. Jiang and R. A. Dougal, "Control design and testing of a novel fuel-cell-powered battery-charging," IEEE APEC'03, vol. 2, pp. 1127-1133, Feb. 2003.
[27] P. Mattavelli, "A modified dead-beat control for UPS using disturbance observers," IEEE PESC'02, vol. 4, pp. 1618-1623, June 2002.
[28] O. Kukrer, "Deadbeat control of a three-phase inverter with an output LC filter," IEEE Transactions on Power Electronics, vol. 11, pp. 16-23, Jan. 1996.
[29] K.P. Gokhale, A. Kawamura, and R.G. Hoft, "Dead beat microprocessor control of PWM inverter for sinusoidal output waveform synthesis," IEEE PESC'85, pp. 28-36, 1985.
[30] F. Botteron, H. Pinheiro, H. A. Grundling, and H. L. Hey, "Digital voltage and current controllers for three-phase PWM inverter for UPS applications," IEEE IAS'01, vol.4, pp. 2667-2674, 2001.
[31] V. Utkin, J. Guldner, and J. Shi, Sliding Mode Control in Electromechanical Systems, Taylor & Franci, Philadelphia, PA, 1999.

Jin-Woo Jung received the B.S and M.S degrees in Electrical Engineering from Hanyang University, Seoul, Korea in 1991 and 1997, respectively and Ph.D. degree in the Department of Electrical and Computer Engineering, The Ohio State University, Columbus,

OH, USA, in 2005. From 1997 to 2000, he worked at Digital Appliance Research Laboratory, LG Electronics Co., Ltd., Seoul, Korea. He is currently working at Corporate R&D Center, Samsung SDI Co., Ltd., Korea. His research interests are in the area of distributed generation systems, fuel cell systems, electric machines, AC motor drives, power converters, and control.

Ali Keyhani is a fellow of IEEE and recipient of the Ohio State University College of Engineering Research Award for 1989, 1999 and 2003. From 1967 to 1972, he worked for Hewlett-Packard Co. and TRW Control. Currently, he is a Professor of Electrical Engineering at the Ohio State University, Columbus, OH. He was the past Chairman of Electric Machinery Committee of IEEE Power Engineering Society and the past editor of IEEE Transaction on Energy Conversion. He is the director of OSU Electromechanical and Mechatronic Systems laboratory. Dr. Keyhani's research activities focus on the control of distributed energy systems, design and modeling of electric machine, control and design of Power Electronic systems, DSP-based virtual test bed for design, control of power systems, automotive systems, modeling, parameter estimation and failure detection systems.